over 0.5×10^{-3} M, no AgI/SiO_2 particles that had AgI single core could be prepared with the *reaction A*.

Silica-coating in *reaction B*. To perform silica coating with the use of TEOS, ethanol is added to AgI colloid. The addition of ethanol varies dielectric constant of the colloid solution, which should affect stability of AgI nanoparticles. According to preliminary TEM observations, the AgI nanoparticles that were surface-modified with MPS were well dispersed in water, and in contrast, aggregation of the MPS-modified AgI particles took place in water/ethanol solution. MPS molecules modified AgI nanoparticle surface with their thiol groups, and consequently silanol groups were introduced onto the surface. Because the dielectric constant of water/ethanol solution is lower than water, silanol groups on the AgI particle surface probably tend to deionize in the water/ethanol solution. Thus, the electrostatic repulsion between the AgI particles was weak in the water/ethanol solution, compared with that in water. Therefore, the aggregates of AgI nanoparticles were generated in the water/ethanol solution.

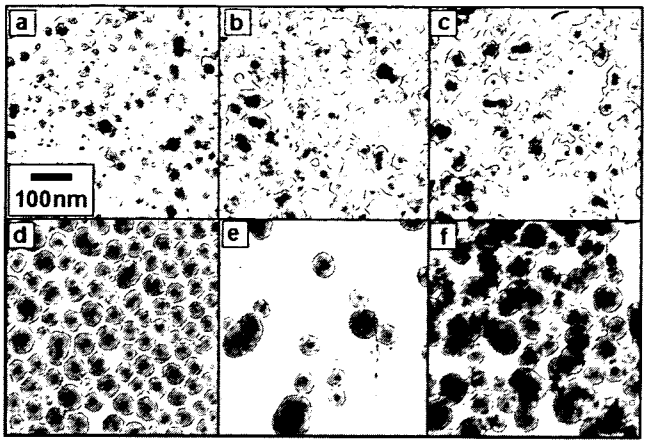

Figure 2. TEM images of AgI/SiO_2 particles prepared at DMA concentrations of (a) 0.002, (b) 0.004, (c) 0.005, (d) 0.01, (e) 0.05 and (f) 0.1 M. Initial concentrations of $AgClO_4$, KI, MPS, water and TEOS were 1.0×10^{-3}, 2.0×10^{-3}, 4.5×10^{-5}, 20 and 0.02 M with respect to the total solution volume.

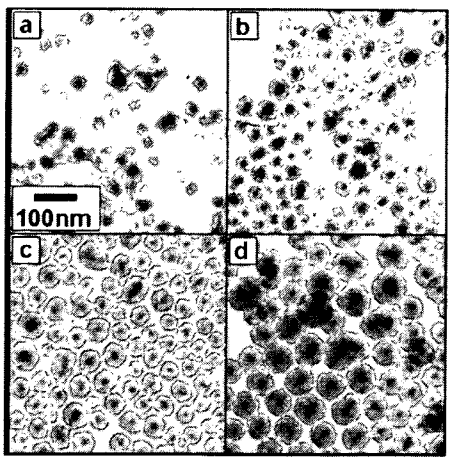

Figure 3. TEM images of AgI/SiO_2 particles prepared at TEOS concentrations of (a) 0.005, (b) 0.01, (c) 0.02 and (d) 0.04 M. Initial concentrations of $AgClO_4$, KI, MPS, DMA and water were 1.0×10^{-3}, 2.0×10^{-3}, 4.5×10^{-5}, 0.01 and 20 M with respect to the total solution volume.

According to the previous work, the AgI nanoparticles were well stabilized in water, compared with in water/ethanol solution. To improve the stability of AgI nanoparticles in sol-gel reaction, silica-coating was performed at high water concentrations. Fig. 2 shows the TEM images of AgI/SiO_2 particles prepared with the use of 20 M water at various DMA concentrations, in which an AgI concentration was 1.0×10^{-3} M. At a DMA concentration of 0.002 M, shell free AgI particles and core-free silica particles were obtained due to a shortage of DMA catalyst. At 0.004 and 0.005 M, though core-free silica particles were obtained, the AgI nanoparticles were coated with silica. At a DMA concentration as high as 0.01 M, only AgI/SiO_2 particles were observed. Addition of DMA is considered to increase the ionic strength of the solution due to the dissociation and catalyzes the hydrolysis and condensation of the alkoxysilanes [17]. Thus, the high DMA concentration should reduce the double layer repulsion between the AgI nanoparticles and the silica nuclei. As a result, the silica nuclei were efficiently deposited on the AgI particle surfaces. At DMA concentrations as high as 0.05 and 0.1 M, particles with AgI particle aggregates were observed, and the shape of the AgI/SiO_2 particles tended to be distorted. At high DMA concentrations, the AgI cores probably aggregated before becoming coated with silica due to the increased ionic strength that would promote AgI particle aggregation.

For the control of shell thickness, TEOS concentration was varied in the experiments of Figs. 3 (a)–(d). At a TEOS concentration as low as 0.005 M (Fig. 3 (a)), many core-free silica particles were generated because of low ionic strength. At TEOS concentrations of 0.01-0.04 M (Figs. 3 (b)–(d)), most of the particles were quasi-perfect core-shells with just one AgI core and the shell thickness increased from 15 to 28 nm. Thus, the TEOS concentration was found to control the silica shell thickness within a certain threshold.

Summary

AgI/SiO_2 particles were prepared by employing a sol-gel reaction of TEOS with DMA catalyst in the presence of MPS-modified AgI nanoparticles for producing AgI/SiO_2 particle colloid. The use of 4.5×10^{-5} M MPS, 20 M water, 0.01 M DMA and 1 mM AgI provided formation of AgI-silica core-shell structure. With an increase in TEOS concentration, the silica shell thickness increased from 15 to 28 nm. Concentration effects can probably be explained by the difference in ionic strength of the solution.

Acknowledgements

This research was partially supported by the Ministry of Education, Culture, Sports, Science and Technology of Japan (Grant-in-Aid for the COE project, Giant Molecules and Complex Systems), and by the Ministry of Health, Labor and Welfare of Japan.

References

[1] L. M. Liz-Marzán, M. Giersig and P. Mulvaney: Chem. Commun. (1996), p. 731

[2] S. M. Marinakos, D. A. Shultz and D. L. Feldheim: Adv. Mater. Vol. 11 (1999), p. 34

[3] V. V. Hardikar and E. Matijevic: J. Colloid Interface Sci. Vol. 221 (2000), p. 133

[4] S. R. Hall, S. A. Davis and S. Mann: Langmuir Vol. 16 (2000), p. 1454

[5] Y. Kobayashi, M. A. Correa-Duarte and L. M. Liz-Marzán: Langmuir Vol. 17 (2001), p. 6375

[6] G. Cho, B. M. Fung, D. T. Glatzhofer, J.-S. Lee and Y.-G. Shul: Langmuir Vol. 17 (2001), p. 456

[7] T. Tago, T. Hatsuta, R. Nagase, M. Kishida and K. Wakabayashi: Kagaku Kogaku Ronbunshu Vol. 27 (2001), p. 288 (in Japanese)

[8] H. Wang, H. Nakamura, Y. Yao, H. Maeda and E. Abe: Chem. Lett. Vol. 30 (2001), p. 1168

[9] Y. Lu, Y. Yin, Z.-Y. Li and Y. Xia: Nano Lett. Vol. 2 (2002) p. 785

[10] C. Graf, D. L. J.Vossen, A. Imhof and A. van Blaaderen: Langmuir Vol. 19 (2003), p. 6693

[11] E. Mine, A. Yamada, Y. Kobayashi, M. Konno and L. M. Liz-Marzán: J. Colloid Interface Sci. Vol. 264 (2003), p. 385

[12] Y. Kobayashi, H. Katakami, E. Mine, D. Nagao, M. Konno and L. M. Liz-Marzán: J. Colloid Interface Sci. Vol. 283 (2005), p. 392

[13] Y. Kobayashi, M. Horie, M. Konno, B. Rodríguez-González and L. M. Liz-Marzán: J. Phys. Chem. B Vol. 107 (2003), p. 7420

[14] M. Giersing, T. Ung, L. M. Márzan and P. Mulvaney: Adv. Mater. Vol. 9 (1997), p. 570

[15] Y. Kobayashi, K. Misawa, M. Takeda, M. Kobayashi, M. Satake, Y. Kawazoe, N. Ohuchi, A. Kasuya and M. Konno: Colloids Surfaces A Vol. 251 (2004), p. 197

[16] Y. Wang, J. Mo, W. Cai, L. Yao and L. Zhang: Mater. Lett. Vol. 56 (2002), p. 502

[17] D. Nagao, Y. Kon, T. Satoh and M. Konno: J. Chem. Eng. Japan Vol. 33 (2000), p. 468

Journal of
Nanoscience and Nanotechnology
Vol. 7, 2690–2695, 2007

Concentrated Colloids of Silica-Encapsulated Gold Nanoparticles: Colloidal Stability, Cytotoxicity, and X-ray Absorption

Yeon-Su Park[1,*], Atsuo Kasuya[1,*], Andriy Dmytruk[1], Noda Yasuto[1], Motohiro Takeda[2], Noriaki Ohuchi[3], Yoshinori Sato[4], Kazuyuki Tohji[4], Motohiro Uo[5], and Fumio Watari[5]

[1]*Center for Interdisciplinary Research, Tohoku University, Aoba-ku, Sendai 980-8578, Japan*
[2]*Department of Bioengineering and Robotics, Tohoku University, Aoba-ku, Sendai 980-8579, Japan*
[3]*Division of Surgical Oncology, Graduate School of Medicine, Tohoku University, Aoba-ku, Sendai 980-8574, Japan*
[4]*Graduate School of Environmental Studies, Tohoku University, Aoba-ku, Sendai 980-8579, Japan*
[5]*Graduate School of Dental Medicine, Hokkaido University, Kita-ku, Sapporo 060-8589, Japan*

As an effort to develop a new, effective, nontoxic X-ray contrast agent, the concentrated colloids of silica-encapsulated gold nanoparticles (Au@SiO_2 NPs) were fabricated and their colloidal stability, cytotoxicity, and X-ray absorption were investigated. The concentrated colloidal NPs were manufactured by forming a 4 nm-thick silica shell on the surface of each Au NP with 15 nm diameter, followed by enrichment to [Au] = 100 mM. They were very stable in water: the NPs were well separated each other without forming agglomerates and their optical property was very similar to that before enrichment. The colloidal stability of the NPs in biological environment was strongly dependent on their previous morphology in water. The NPs with minor shell damage were stable in phosphate buffered saline (PBS) solution: both in water and in PBS solution, they showed very similar morphology and optical property. However, the NPs with profound shell damage formed big agglomerates in PBS solution, resulting in the red-shift and broadening of the Au surface plasmon resonance peak. Cell viability and proliferation assessments revealed the biocompatibility of the Au@SiO_2 NPs: no apparent cytotoxicity was observed even at 100 ppm NPs. The concentrated colloidal NPs showed very strong X-ray absorption. Their relative X-ray transmittance to water was comparable to that of a commercial agent. Considering these, the concentrated colloids of the Au@SiO_2 NPs are suitable for an X-ray contrast agent.

Keywords: Gold, Silica, X-ray Absorption, Cytotoxicity, Colloidal Stability.

1. INTRODUCTION

As concerns on human health increase tremendously in modern society, there have been strong demands for more effective and safer medical diagnoses. One of the most indispensable modern diagnostic tools is a computed tomography (CT), which strongly relies on the contrast ability of X-ray contrast agents. Currently, tri-iodobenzene derivatives are extensively used as the contrast agents. However, sometimes these iodine-containing small organic molecules cause some serious problems such as limited imaging time, due to their short vascular circulation time, and renal toxicity. Thus, CT practices occasionally require intra-arterial catheterization which may impose serious health risks. In these regards, there have been ceaseless efforts to develop more effective and safer X-ray contrast agents.[1–5] Most of them have focused on the modification of iodine-containing contrast molecules: encapsulation in[1–4] or linkage to[5] biocompatible organic molecules/polymers. A recent report by Hainfeld et al., however, demonstrated a possibility of Au NPs for an X-ray contrast agent.[6] They obtained the contrast images of the blood vessels and some organs of mice, by utilizing concentrated colloids of 1.9 nm diameter Au NPs as an X-ray contrast agent.

The nontoxic nature of bulk Au and relatively large (e.g., a few nm or bigger in diameter) Au NPs has been well documented,[7,8] but investigations on the toxicity of small Au NPs have been scarce. Recently, Schmit et al. reported the toxicity of very small Au NPs.[9,10] The authors observed strong cytotoxicity from 1.4 nm Au NPs, of which size is in a range for deteriorative interaction with

*Authors to whom correspondence should be addressed.

1533-4880/2007/7/2690/006 doi:10.1166/jnn.2007.601

the major grooves of deoxyribonucleic acids (DNAs). Thus, for medical applications, it is highly desirable to use the Au NPs larger than DNA grooves (typically less than 2 nm). In addition to the cytotoxicity problem, the Au NPs commensurate with or smaller may cause poor X-ray contrast because of their short vascular circulation time. However, very large Au NPs are also undesirable for medical applications because of the colloidal stability of the NPs decreasing with size and the difficulty in preparing homogeneous large (e.g., 40 nm or bigger in diameter) Au NPs.[11] Taking these into account, relatively large (here, between 10 and 40 nm in diameter) Au NPs seem to be suitable for an X-ray contrast agent application.

Like many medical applications of other colloidal NPs, the application of colloidal Au NPs for an X-ray contrast agent requires them being in a highly concentrated state to ensure high X-ray contrast. However, it is not a trifle to prepare stable and concentrated colloids of relatively large Au NPs, without proper surface modifications, because of their strong tendency to coagulate in concentrated state. One of the most useful and bio-friendly surface modifications is to encapsulate each Au NP in a silica shell because silica is biocompatible, feasible for further surface modifications,[8,12–14] and has strong negative charge in biological environment.[15] The strong negative charge on the silica surfaces, contributing to electrostatic repulsion among the NPs, may enable to prepare highly stable and concentrated colloids of relatively large Au NPs.

There has been sparse documentation[16] on the concentrated colloids of silica-encapsulated Au ($Au@SiO_2$) NPs, even though plenty of documents[12,17–22] have been available on the morphology and optical property of the NPs and their assemblies prepared from relatively low precursor concentration without enrichment. Unfortunately, no documentation is available on the colloidal stability and cytotoxicity of $Au@SiO_2$ NPs in biological environment, which are essential factors for medical applications. Here, as an effort to develop a new class of an effective and safe X-ray contrast agent, we report the colloidal stability in biological environment, *in vitro* cytotoxicity, and X-ray absorption of the concentrated colloidal $Au@SiO_2$ NPs (Au core diameter = ca. 15 nm, silica shell thickness = ca. 4 nm), along with their morphology and optical property.

2. EXPERIMENTAL DETAILS

2.1. Materials

Hydrogen tetrachloroaurate(III) tetrahydrate ($HAuCl_4 \cdot 4H_2O$), trisodium citrate dehydrate (Na_3-Cit), formaldehyde, 0.1 M phosphate buffered saline (PBS) solution were purchased from Wako Pure Chemicals. 3-Aminopropyl trimethoxysilane (APS) was supplied by Alfa-Aesar. Sodium silicate solution (ca. 27% SiO_2), DOWEX® 50WX4-400 ion-exchange resin, alpha-Minimum Essential Medium (MEM), and fetal bovine serum (FBS) were acquired from Sigma-Aldrich. Trypan blue and alamarBlue™ were provided by Gibco and Biosource, respectively. All chemicals were used as received. Milli-Q water (>18.2 MΩ cm) was used to prepare all aqueous solutions.

2.2. Preparation

The colloids of citrate-stabilized Au NPs were prepared according to the previously reported procedure.[11,16] Briefly, 15 ml of mildly heated 1% Na_3-Cit solution was added to 282 ml of boiling 0.532 mM $HAuCl_4 \cdot 4H_2O$ solution under stirring: the final concentrations of Au^{3+} and $citrate^-$ were 0.5 and 0.17 mM, respectively. Silica shells were formed by adding 0.75 ml of 1 mM APS solution and 12 ml of 0.54 wt% sodium silicate solution (pH = 10.5–11, adjusted by using DOWEX® 50WX4-400 ion-exchange resin) to 300 ml of the colloids of citrate-stabilized Au NPs, followed by standing the mixtures (pH ≅ 8.5) for three days.[14,16,17,21] The resulting colloids of $Au@SiO_2$ NPs were cleaned by a series of washing cycle: centrifugation (25,000 × g, 15 minutes), supernatant removal, and redispersion in water. Concentrated colloids were prepared by repeating the washing cycle, while gradually decreasing the amount of water for redispersion in each cycle (hereafter, referred as a 'mild enrichment'). A typical mild enrichment consisted of 4 washing cycles. Assuming that all Au^{3+} ions were used for producing Au NPs, the concentration of metallic Au in the concentrated colloids was 100 mM, 200 times higher than that in the colloids before the enrichment. Twice repetition of the mild enrichment was also performed to investigate its influence on the morphology and optical properties of the NPs. In this case, the final concentration of metallic Au in the resulting colloidal solution was also adjusted to 100 mM. For convenience, the metallic Au concentration was used for representing the concentration of Au or $Au@SiO_2$ NPs in colloids.

2.3. Instrument and Characterization

For characterizing the morphology of the NPs, the transmission electron microscopy (TEM) was performed with a JEOL JEM-2000 microscope operating at 200 KeV. The optical property of the colloidal NPs was characterized from their visible absorption spectra obtained with a Hitach U-2000 spectrophotometer. All optical spectra were obtained after adjusting metallic Au concentration to 0.5 mM. A Rigaku Rotaflex X-ray spectrometer was used for measuring X-ray transmittances of samples.

The stability of the concentrated colloidal NPs in biological environment was characterized based on the changes in their morphology and optical property upon transferring to 0.1 M PBS solution. The volume ratio of the colloid to the PBS solution was set to 0.5.

The viability and proliferation of rat fibroblast MC3T3-E1 cells, assessed by using a almarBlue™ assay, were used for evaluating the cytotoxicity of the NPs. For cell viability tests, the rat fibroblasts were incubated at 37° in 24-well plates using alpha-MEM containing 10% FBS (10^4 cells per well) and then various amount of the NPs (0.01–100 ppm) in water were added to each well. After further incubation at 37° for 24 hours, the viability of the rat fibroblasts was estimated based on the calorimetric detection of almarBlue™ reduction caused by live cells. For cell proliferation assays, both the rat fibroblasts and the NPs in water were seeded onto 24-well plates using alpha-MEM containing 10% FBS (10^4 cells per well) and then co-incubated for 24 hours. After cell fixing with formaldehyde and staining with trypan blue, stained cells (live cells) were counted under an optical microscope. In both the tests, the control sample was rat fibroblast MC3T3-E1 cells.

3. RESULTS AND DISCUSSION

3.1. Morphology

The citrate-induced reduction of Au^{3+} produced homogeneous spherical Au NPs with ca. 15 nm in diameter (Fig. 1(a)). The $Au@SiO_2$ NPs, prepared through silica coating in the basic silicate solution, are well separated each other without forming agglomerates, as shown in Figure 1(b). They have relatively homogeneous spherical silica shells of which thickness is ca. 4 nm.

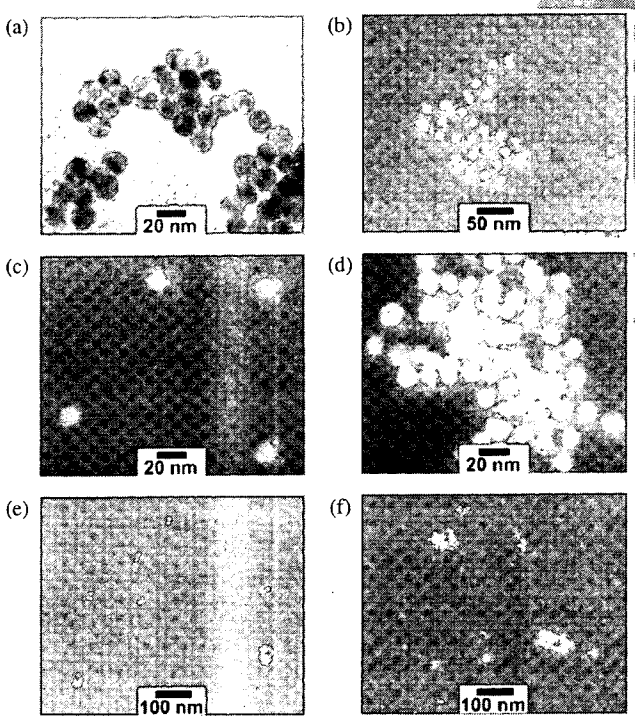

Fig. 1. TEM images of Au and $Au@SiO_2$ nanoparticles: (a) citrate-capped Au, (b) as-prepared $Au@SiO_2$ in water, (c) $Au@SiO_2$ in water after mild enrichment, (d) $Au@SiO_2$ after twice repetition of mild enrichment, (e) $Au@SiO_2$ in 0.1 M PBS solution after mild enrichment, and (f) $Au@SiO_2$ in 0.1 M PBS solution after twice repetition of mild enrichment. The concentrations of the NPs before and after the enrichments were equivalent to 0.5 and 100 mM metallic Au, respectively.

The concentrated colloidal $Au@SiO_2$ NPs, prepared through the mild enrichment, are well separated each other without forming agglomerates, even though some silica shells have minor shell damage such as detachment of some silica (Fig. 1(c)). The stability of these concentrated colloidal $Au@SiO_2$ NPs with minor shell damage (MSD) can be attributed to their high surface charge. In the experimental conditions of near neutral pH, the silica surfaces have high negative charge owing to the low isoelectric point of silica.[15] This enhances electrostatic repulsion among the NPs enough to stabilize them in the concentrated state.

The repetition of the mild enrichment exerted detrimental effect on the morphology of the $Au@SiO_2$ NPs. As shown in Figure 1(d), twice repetition of the enrichment resulted in profound shell damage (PSD): the silica shells seem to be inhomogeneous and little compact, compared with those obtained through the typical mild enrichment process; in part, they are loosely distributed among the Au NPs. Most of the NPs with PSD are poorly separated each other. In many cases, each NP is closely contacting with its immediate neighbor NPs through very thin silica barrier. Some NPs partially expose their Au cores or have big cores compose of two or more Au NPs. The formation of the big cores is related with the coagulation of the NPs with no or little silica. They have surface charge insufficient to prevent them from coagulation, because their surface charge diminishes with decreasing silica surface area.

3.2. Optical Property

As shown in Figures 2(a) and (b), the formation of 4 nm-thick silica shells caused a shift of Au surface plasmon resonance (SPR) peak from 519 to 523 nm. This red-shift by 4 nm is due to an increase in the local refractive index of the surrounding medium[17, 22] and is well in accordance with previous reports.[16, 17]

The optical property of the $Au@SiO_2$ NPs was strongly dependent on their morphology. As shown in Figure 2(c), the NPs with MSD show a SPR peak of which shape, intensity, and position are very similar to those of the NPs before the enrichment (Fig. 2(b)). The SPR peak of the NPs with PSD in Figure 2(d), however, is somewhat broad, weak, and red-shifted by 3 nm, compared with that of the NPs with MSD. These slight changes in optical property can be attributed to the close contact of the NPs and the existence of the NPs with bigger Au core.

3.3. Colloidal Stability in Biological Environment

In biological environment, the concentrated colloidal $Au@SiO_2$ NPs formed agglomerates of which size was strongly dependent on their initial morphology in water.

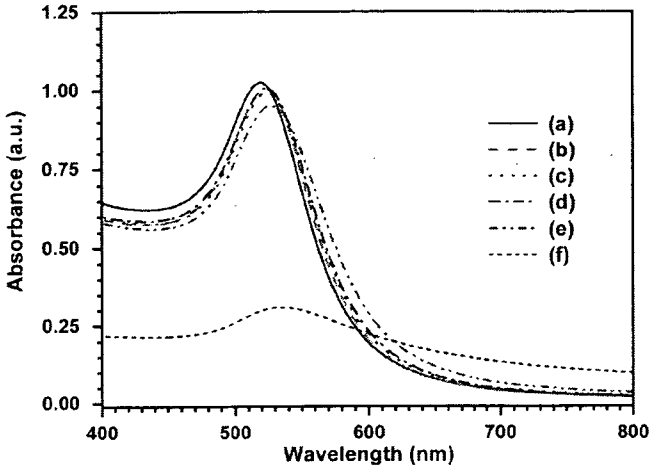

Fig. 2. Visible absorption spectra of Au and Au@SiO_2 nanoparticles: (a) citrate-capped Au, (b) as-prepared Au@SiO_2 in water, (c) Au@SiO_2 in water after mild enrichment, (d) Au@SiO_2 after twice repetition of mild enrichment, (e) Au@SiO_2 in 0.1 M PBS solution after mild enrichment, and (f) Au@SiO_2 in 0.1 M PBS solution after twice repetition of mild enrichment.

As shown in Figure 1(e), the morphology of the NPs with MSD in the PBS solution is very similar to that of the corresponding NPs in water, except for some agglomerates composed of relatively small number of the NPs. The formation of slightly more and bigger agglomerates of the NPs in the PBS solution is related with the flocculation caused by an increase in the ionic strength of the solution. Due to its high ion concentration, the PBS solution has stronger ionic strength than water. As the ionic strength of a solution increases, charge (opposite in sign) density around NPs increases. Because both ionic strength and charge density are inversely proportional to the square of the Debye shielding length, which is a measure of the strength of electrostatic potential damping from its pure value, electrostatic repulsion among the NPs is reduced and hence the NPs are destabilized with increasing ion concentration. Unlike those with MSD, the concentrated colloidal Au@SiO_2 NPs with PSD were unstable in the PBS solution: an immediate formation of precipitates was observed upon transferring to the solution. As shown in Figure 1(f), the TEM images of the NPs with PSD in the PBS solution show big agglomerates, along with some single NPs and small agglomerates composed of a few NPs with little or no silica shell. The big agglomerates consist of a few tens of the NPs, in which a couple of bigger Au NP cores are included. As discussed earlier, the formation of the big agglomerates of the NPs with PSD is related with the ionic strength of the PBS solution.

The optical property of the Au@SiO_2 NPs in PBS solution was also strongly influenced by their initial morphology: the NPs with MSD showed little change, whereas those with PSD experienced drastic change. The visible absorption spectrum of the NPs with MSD in the PBS solution (Fig. 2(e)) is very similar to that of the corresponding NPs in water (Fig. 2(c)): there is little difference in the shape, intensity, and position of the Au SPR peak. However, as shown in Figure 2(f), the NPs with PSD in the PBS solution shows a broad and weak Au SPR peak with very large background, compared with those in water (Fig. 2(d)). And their SPR peak is located at 534 nm, which is 7 nm longer than that in water. These optical observations imply the existence of various sizes of bigger NPs in the PBS solution and are well coincided with the previously described microscopic observations.

3.4. Cytotoxity

For medical applications, the Au@SiO_2 NPs should be biocompatible. Their biocompatibility was evaluated based on the viability and proliferation of rat fibroblast MC3T3-E1 cells. In general, 50% cell viability (or proliferation) is considered as a border of live or dead cells: materials giving 50% or higher cell viability (or proliferation) are biocompatible, while those with lower than 50% values are toxic. Figure 3 shows the viability and proliferation of the rat fibroblast cells after 24 hours incubation. In all the NP concentrations tested here, the rat fibroblast cells show more than 50% viability and proliferation. Even at a very high NP concentration of 100 ppm, the cell viability and proliferation are more than 70 and 60%, respectively. These confirm the biocompatibility of the Au@SiO_2 NPs. Especially the NPs show excellent biocompatibility at the concentration of 1 ppm or lower, as can be inferred from near 100% cell viability and proliferation.

3.5. X-ray Absorption

For achieving high X-ray contrast, contrast agents should show much stronger X-ray absorption (so, much lower X-ray transmittance) than human body, because X-ray contrasting ability relies on the differences in their X-ray

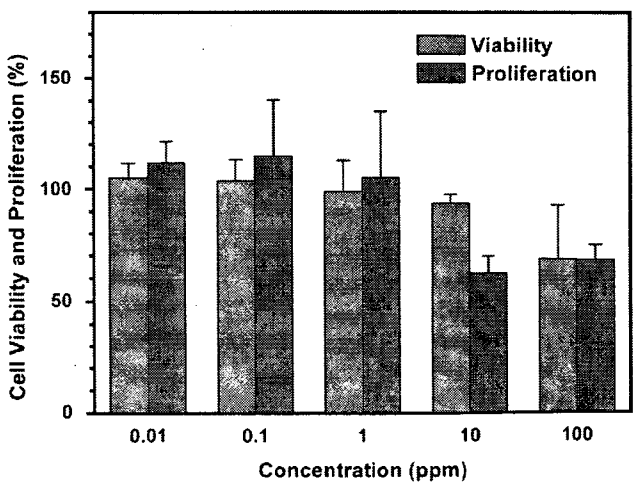

Fig. 3. Viability and proliferation of rat fibroblast MC3T3-E1 cells at various concentrations of Au@SiO_2 nanoparticles.

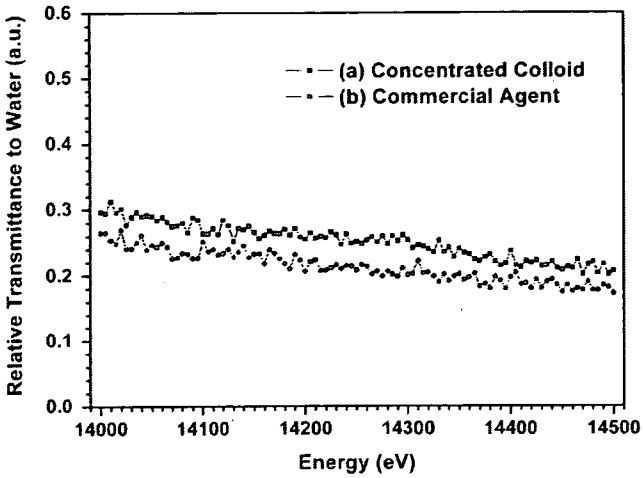

Fig. 4. Relative X-ray transmittances of (a) the concentrated colloid of $Au@SiO_2$ nanoparticles ([Au] = 100 mM) and (b) a commercial X-ray contrast agent (Iopamiron® 300). Relative transmittance = transmittance of sample/transmittance of water.

absorption. Therefore, the relative X-ray transmittance of a sample to water (a major constituent of human body) is a very very important factor for evaluating its contrast ability. In general, materials with lower relative X-ray transmittance give better X-ray contrast.

Figure 4 shows the relative X-ray transmittances of the 100 mM colloidal $Au@SiO_2$ NPs and a commercial X-ray contrast agent (Iopamiron® 300). Average relative transmittance of the colloidal NPs is close to that of the commercial contrast agent. At Au L_I edge, the colloidal NPs shows the relative transmittance of ca. 0.237, which is very close to the calculated value of 0.231 based on X-ray mass attenuation coefficient of Au. Their slight discrepancy may be mainly due to the loss of the NPs during enrichments. Considering very low relative X-ray transmittance, comparable to that of a commercial contrast agent, the concentrated colloidal $Au@SiO_2$ NPs may be suitable for an X-ray contrast agent application.

4. SUMMARY AND CONCLUSIONS

As an effort to develop a new class of an effective and nontoxic X-ray contrast agent, highly concentrated colloidal $Au@SiO_2$ NPs were prepared and their colloidal stability in biological environment, *in vitro* cytotoxicity, and X-ray absorption were investigated. Each NP consists of ca. 15 nm diameter Au core and ca. 4 nm thick silica shell. The concentration of the concentrated colloidal NPs was equivalent to 100 mM metallic Au.

Highly stable and concentrated colloidal $Au@SiO_2$ NPs with MSD were prepared through the mild enrichment. The colloidal NPs with MSD were morphologically stable in concentrated state: they were well-separated each other, without forming agglomerates. The optical property of the concentrated colloidal NPs with MSD was very similar to that of the colloidal NPs before the enrichment: there was little change in the shape, intensity, and position of Au SPR peaks before and after the enrichment.

The concentrated colloidal $Au@SiO_2$ NPs with PSD were prepared through the repetition of the mild enrichment. The concentrated colloidal NPs with PSD showed the morphology somewhat different from that of the concentrated colloidal NPs with MSD: they were poorly separated each other and had very close contact with neighbor NPs. Due to their morphology, the NPs with PSD showed a Au SPR peak which is slightly broad, weak, and red-shifted as compared with that of the NPs with MSD.

In biological environment, the stability of the concentrated colloidal $Au@SiO_2$ NPs was strongly dependent on their previous morphology in water. The concentrated colloidal NPs with MSD were stable in PBS solution, even though some small agglomerates were formed. However, the concentrated colloidal NPs with PSD were unstable in PBS solution: they formed big agglomerates, resulting in precipitation. These morphological differences affected their optical property. The colloidal NPs with MSD in PBS solution showed the Au SPR peak similar to that of the NPs in water, whereas those with PSD showed a very broad and red-shifted peak in PBS solution, as compared with those in water.

The $Au@SiO_2$ NPs are biocompatible. Both cell viability and proliferation assessments revealed no apparent cytotoxicity of the NPs even at the highest NP concentration tested here (100 ppm). Especially, at 1 ppm or lower, the NPs have an excellent biocompatibility: they showed near 100% cell viability and proliferation.

The concentrated colloidal $Au@SiO_2$ NPs showed strong X-ray absorption. Their relative transmittance to water, being inversely proportional to their X-ray contrast ability, is very low and close to that of a commercial contrast agent.

Taking into account their high colloidal stability in biological environment, excellent biocompatibility, and relative X-ray transmittance comparable to a commercial agent, the concentrated colloids of the $Au@SiO_2$ NPs, with relatively large Au core and little (or no) silica shell damage, are excellent materials for X-ray contrast agents.

Acknowledgments: This work was partially supported by Grant-in-Aid from the Ministry of Education, Science, Sports, and Culture, Japan. Authors wish to thank Prof. M. Konno of Tohoku University for his generosity in using the centrifuge.

References and Notes

1. U. P. Schmiedl, W. Krause, J. Leike, and A. Sachse, *Acad. Radiol.* 6, 164 (1999).
2. V. P. Torchilin, *Adv. Drug Deliv. Rev.* 54, 235 (2002).
3. D. R. Vera and R. F. Mattrey, *Acad. Radiol.* 9, 784 (2002).
4. C.-Y. Kao, E. A. Hoffman, K. G. Beck, R. V. Bellamkonda, and A. V. Annapragada, *Acad. Radiol.* 10, 475 (2003).
5. V. P. Torchilin, M. D. Frank-Kamenetsky, and G. L. Wolf, *Acad. Radiol.* 6, 61 (1999).

6. J. F. Hainfeld, D. N. Slatkin, T. M. Focella, and H. M. Smilowitz, *Br. J. Radiol.* 79, 248 (**2006**).
7. E. E. Connor, J. Mwamuka, A. Gole, C. J. Murphy, and M. D. Wyatt, *Small* 1, 325 (**2005**).
8. Z. P. Xu, Q. H. Zeng, G. Q. Lu, and A. B. Yu, *Chem. Eng. Sci.* 61, 1027 (**2006**).
9. Y. Liu, W. Meyer-Zaika, S. Franzka, G. Schmid, M. Tsili, and H. Kuhn, *Angew. Chem., Int. Ed.* 42, 2853 (**2003**).
10. M. Tsoli, H. Kuhn, W. Brandau, H. Esche, and G. Schmid, *Small* 1, 841 (**2005**).
11. G. Frens, *Nat. Phys. Sci.* 241, 20 (**1973**).
12. E. Mine, A. Yamada, Y. Kobayashi, M. Konno, and L. M. Liz-Marzán, *J. Colloid Interf. Sci.* 264, 385 (**2003**).
13. T. Schiestel, H. Brunner, and G. E. M. Tovar, *J. Nanosci. Nanotechnol.* 4, 504 (**2004**).
14. B. Rodríguez-González, A. Sánchez-Iglesias, M. Giersig, and L. M. Liz-Marzán, *Faraday Discuss.* 125, 133 (**2004**).
15. X. Cui, W.-C. Zin, W.-J. Cho, and C.-S. Ha, *Mater. Lett.* 59, 2257 (**2005**).
16. Y.-S. Park, L. M. Liz-Marzán, A. Kasuya, Y. Kobayashi, D. Nagao, M. Konno, S. Mamykin, A. Dmytruk, M. Takeda, and N. Ohuchi, *J. Nanosci. Nanotechnol.* 6, 3503 (**2006**).
17. L. M. Liz-Marzán, M. Giersig, and P. Mulvaney, *Langmuir* 12, 4329 (**1996**).
18. F. Caruso, M. Spasova, V. Salgueiriño-Maceria, and L. M. Liz-Marzán, *Adv. Mater.* 13, 1090 (**2001**).
19. F. García-Santamaría, V. Salgueiriño-Maceria, C. López, and L. M. Liz-Marzán, *Langmuir* 18, 4519 (**2002**).
20. Y. Yang, M. Hori, T. Hayakawa, and M. Nogami, *Surf. Sci.* 579, 215 (**2005**).
21. I. Tunc, S. Suzer, M. A. Correa-Duarte, and L. M. Liz-Marzán, *J. Phys. Chem. B* 109, 7597 (**2005**).
22. S. Liu and M. Han, *Adv. Funct. Mater.* 15, 961 (**2005**).

Received: 25 October 2006. Revised/Accepted: 22 November 2006.

Journal of
Nanoscience and Nanotechnology
Vol. 7, 3750–3753, 2007

Aqueous-Phase Synthesis of Ultra-Stable Small CdSe Nanoparticles

Yeon-Su Park[1,*], Andriy Dmytruk[1], Igor Dmitruk[1], Noda Yasuto[1], Atsuo Kasuya[1,*], Motohiro Takeda[2], and Noriaki Ohuchi[2]

[1]Center for Interdisciplinary Research, Tohoku University, Aoba-ku, Sendai 980-8578, Japan
[2]Division of Surgical Oncology, Graduate School of Medicine, Tohoku University, Aoba-ku, Sendai 980-8574, Japan

Very stable and small CdSe nanoparticles (NPs) were synthesized from the aqueous solutions containing L-cysteine (Cys) at room temperature. The Cys-capped CdSe NPs showed a very sharp excitonic peak at 420 nm. Its very small full width at half maximum (18 nm) indicates very high quality of the CdSe NPs. Their absorption features experienced little change over a month, implying an excellent stability of the CdSe NPs. The synthesis conditions were very critical to the optical property and stability of the CdSe NPs: only those prepared at specific conditions ($n_{Se\text{-}precursor}/n_{Cd\text{-}precursor}$ = 0.25–0.5, $n_{Cys}/n_{Cd\text{-}precursor}$ = ~9, pH = 12) showed very sharp absorption peaks and maintained an excellent stability against time. Under these conditions, the peaks always appear at nearly the same wavelength, indicating that these NPs are selectively stable and grow at a particular size and structure.

Keywords: CdSe, Nanoparticle, Cysteine, Aqueous, Synthesis.

1. INTRODUCTION

Historically, colloidal chemistry has been extensively employed for synthesizing CdSe NPs. Especially, the so-called 'tri-n-octylphosphine (TOP)/tri-n-octylphosphine oxide (TOPO) synthesis' has been widely adapted for producing small CdSe NPs with a relatively narrow size distribution. In the TOP/TOPO synthesis, first introduced by Bawendi et al.,[1] CdSe NPs are synthesized from organometallic precursors in hot nonaqueous TOP/TOPO solutions under inert atmosphere. Since then, numerous modifications of the synthesis have been done to produce CdSe NPs with appropriate sizes and properties.[2–7]

The reverse micelle synthesis also has been largely used for synthesizing small CdSe NPs at mild conditions since the first successful application by Brus et al.[8] They prepared CdSe NPs with 1–10 nm in diameter by adding Cd precursors into the AOT (bis(2-ethylhexyl) sulfosuccinate)/Water/Heptane microemulsion. Various modifications on the reverse micelle synthesis have been done to manufacture CdSe NPs with desired properties.[9,10] Especially, the use of amines as stabilizer molecules allowed to produce very small magic clusters of CdSe showing very sharp and intense absorption peaks.[10]

As the importance of aqueous phase applications increases, there have been some investigations to synthesize water-soluble CdSe NPs. Major efforts have been focused on the surface modification of the CdSe NPs stabilized in hydrophobic organic solvents: water-solubility of the NPs was typically achieved by ligand exchange.[3,11–13] A typical ligand exchange procedure includes either (i) the replacement of hydrophobic capping molecules with hydrophilic molecules in an aqueous alcoholic solution, followed by purification through precipitation and redispersion of the resulting NPs[11,12] or (ii) the removal of hydrophobic capping molecules using alcohols or other organic solvents, resulting in precipitation of unprotected NPs, followed by re-capping of the unprotected NPs with desired hydrophilic capping molecules.[13] However, the ligand exchange procedures are complicated and include a precipitation process, which may alter the physicochemical properties of the NPs.

Recently, an aqueous phase synthesis of CdSe NPs has gained great attention,[14–17] because it can be relatively simple and may not require ligand exchange procedures for achieving water-solubility of the NPs. For the aqueous phase synthesis, it is essential to use water-soluble capping molecules upon preparation. Proper capping of intrinsically hydrophobic CdSe surfaces with hydrophilic molecules can provide them with high stability in aqueous phases. Rogach et al.[14] synthesized CdSe NPs with ca. 1.4–3.2 nm in diameter from aqueous solutions and showed a capping molecule-dependent

*Authors to whom correspondence should be addressed.

1533-4880/2007/7/3750/004 doi:10.1166/jnn.2007.006

size change: thioalcohols resulted in smaller size than thioacids. Yang et al.[15] reported synthesis of CdSe NPs with ca. 3 nm in diameter from aqueous solutions containing poly(vinylpyrrolidone) as capping molecules. Zhou et al. synthesized CdSe NPs with 2.3 and 3.4 nm in diameter from aqueous solutions containing citrate ions[16] and nitrilotriacetate ions,[17] respectively. However, the CdSe NPs synthesized from aqueous solutions showed very broad absorption features, as compared with those prepared from organic phases, implying their wide size distribution.

There has been no report on the aqueous phase-synthesized small CdSe NPs with sharp absorption features comparable to the NPs with hydrophobic capping molecules. Here, we report aqueous phase synthesis of water-soluble, very stable, extremely small CdSe NPs with a very sharp absorption peak. They were produced form basic aqueous solutions containing L-cysteine (Cys) as hydrophilic capping molecules at room temperature under ambient atmosphere. Investigations for the optimization of synthesis conditions, long-term stability, and optical properties of the NPs are presented.

2. EXPERIMENTAL DETAILS

Cadmium sulfate ($CdSO_4 8/3\ H_2O$), sodium sulfite (Na_2SO_3), selenium (Se) powder, 1 N sodium hydroxide (NaOH), and L-cysteine ($HSCH_2CH(NH_2)CO_2H$) were purchased from Wako Pure Chemicals (Japan) and used as received. All aqueous solutions were prepared with deionized H_2O (Milli-Q water, R > 18.2 MΩcm).

Sodium selenosulfate (Na_2SeSO_3) solution was typically prepared by adding 1.00 gram of Se powder and 4.78 grams of Na_2SO_3 into 250 mL of deionized H_2O under magnetic stirring. The mixture solution was heated up to 90 °C and maintained the temperature at least 24 hours under magnetic stirring and darkness. The resulting Na_2SeSO_3 solution was kept under the same conditions and used within 4 days.

Cys-capped CdSe NPs were synthesized by the sequential addition of the desired amounts of NaOH (1 N), Cys, $CdSO_4 8/3H_2O$ (0.15 M), and Na_2SeSO_3 (0.05 M) into deionized H_2O at room temperature under magnetic stirring and ambient atmosphere. Typical concentrations in preparation solutions were $[Cd^{2+}] = 1.5$, $[Se^{2-}] = 0.375$–3.0, [Cys] = 13.2, [NaOH] = 37.5 mM. Resulting colloidal solutions were kept at room temperature under magnetic stirring and darkness. For convenience, 'Se/Cd molar ratio' and 'Cys/Cd molar ratio' were used to represent 'Se-/Cd-precursor molar ratio' and 'Cys/Cd-precursor molar ratio' in preparation solutions, respectively. For the simplicity, number of days is used to represent the duration of reaction (or storage) from the point of the addition of the last chemical (Se-precursor).

Optical absorption spectra were taken with a Hitachi U-2000 spectrophotometer.

3. RESULTS AND DISCUSSION

3.1. Effect of the Amount of Stabilizer Molecules

For optimization of the amount of Cys, different amounts of Cys were dissolved in preparation solutions, while maintaining Se/Cd molar ratio at 0.50. Figure 1 shows a collection of the sharpest absorption spectra for Cys-capped CdSe NPs synthesized at a series of different Cys/Cd molar ratios. The CdSe NPs prepared at the ratio of 2.2 shows a broad first excitonic peak at 414 nm after 3 hour-storage. The peak was then broadened and red-shifted as storage time increases up to 16 days. Further storage of the NPs resulted in the formation of precipitates. These observations insinuate that the Cys/Cd molar ratio of 2.2 is insufficient to stabilize NPs. The CdSe NPs synthesized at the ratio of 4.4 shows a sharpest first excitonic peak at 420 nm after 4 day-storage, which was then gradually decreased and broadened with storage time. The CdSe NPs synthesized at the ratio of 8.8 shows a sharpest first excitonic peak at 420 nm after 6 day-storage: its full width at half maximum (FWHM) is 18 nm, which is extremely small compared with that for the NPs with the size distribution as small as 5%. The excitonic peak experienced little change in position and sharpness up to 1 month of storage, suggesting the formation of the very stable NPs at the ratio of 8.8. The CdSe NPs prepared at the ratio of 17.7 show a sharpest first excitonic peak (FWHM = 19 nm) at 420 nm after 3 hour-storage, which was then gradually decreased and broadened with increasing storage time. Those prepared at the ratio of 35.2 shows a broad first excitonic peak at 418 nm after 3 hour-storage. They then experienced the red-shift and broadening of the peak with increasing storage time. Considering the sharpness and storage time-dependent stability of the first excitonic peak, Cys/Cd molar ratio near 8.8 seems to be optimal for

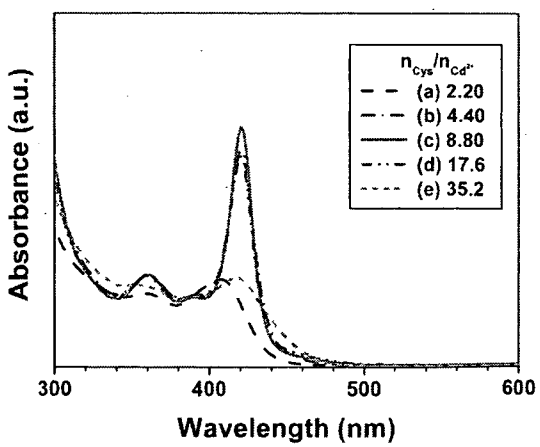

Fig. 1. Sharpest and most intense absorption spectra for Cys-capped CdSe NPs prepared at a series of different Cys/Cd molar ratios: (a) 2.20 (3 hours), (b) 4.40 (4 days), (c) 8.80 (6 days), (d) 17.6 (3 hours), and (e) 35.2 (3 hours). The time in each parenthesis represents sample storage time. Se/Cd ratio = 0.50.

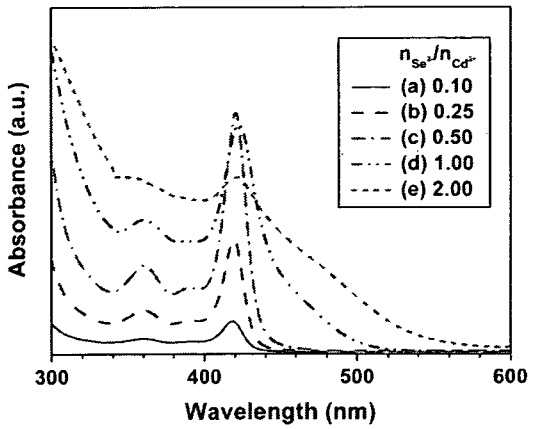

Fig. 2. Sharpest and most intense absorption spectra for Cys-capped CdSe NPs prepared at a series of different Se/Cd molar ratios: (a) 0.10 (2 days), (b) 0.25 (8 days), (c) 0.50 (8 days), (d) 1.00 (2 days), and (e) 2.00 (1 day). The time in each parenthesis represents sample storage time. Cys/Cd molar ratio = 8.8.

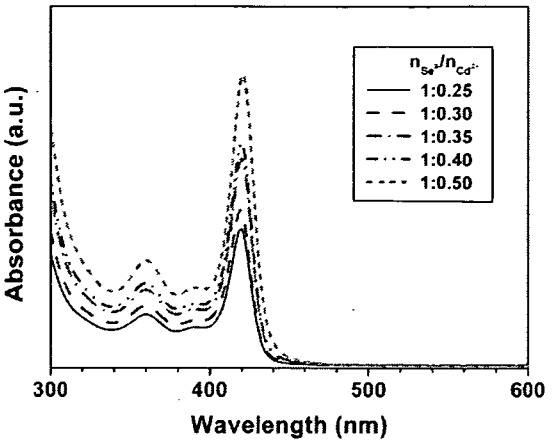

Fig. 3. Evolution of absorption spectra for Cys-capped CdSe NPs as a function of Se/Cd molar ratio. Storage time = 8 days. Cys/Cd molar ratio = 8.8.

the preparation of Cys-capped CdSe NPs in our synthetic conditions.

3.2. Influence of Se-/Cd-Precursor Molar Ratio

For the optimization of Se/Cd molar ratio, Cys-capped CdSe NPs were prepared at various Se/Cd molar ratios, while maintaining the Cys/Cd molar ratio at 8.8, and their absorption spectra were obtained. Figure 2 shows the sharpest absorption spectra for the NPs synthesized at a series of different Se/Cd molar ratios between 0.10 and 2.00. The CdSe NPs prepared at the ratio $\leq$0.50 show a sharp first excitonic peak around 420 nm of which intensity increases, due to the difference of Se-precursor (a limiting reagent) concentration in preparation solutions, with increasing the ratio. FWHM values for the excitonic peak of the NP synthesized at the ratios of 0.10, 0.25, and 0.50 are as small as 19, 18, and 18 nm, respectively. However, the Cys-capped CdSe NPs manufactured at the ratio >0.50 exhibit a very broad first excitonic peak which becomes much broader with increasing the ratio, suggesting the formation of the large NPs with a wide size distribution, as compared with those prepared at the ratio $\leq$0.50.

For the fine tune of Se/Cd molar ratios, Cys-capped CdSe NPs were synthesized at different Se/Cd molar ratios between 0.25 and 0.50 and their absorption spectra were obtained. As shown in Figure 3, the position (420 nm) and FWHM (18 nm) for the first excitonic peak experience practically no change in the Se/Cd molar ratio range, indicating that these NPs are selectively stable and grow at a particular size and structure.

Surprisingly, the spectral features for our Cys-capped CdSe NPs, prepared and stabilized in aqueous solutions, are very similar to those for the magic clusters of CdSe NPs capped by hydrophobic molecules and stabilized in organic solvents: Murray et al.,[1] Kasuya et al.,[10] and Ptatschek et al.[18] reported very similar spectral features for the magic clusters of CdSe NPs capped with TOP/TOPO, dodylamine, and 3-aminopropyltriethoxy silane, respectively, they estimated the sizes of their NPs to be ca. 1.2, 1.5, and 1.7 nm in diameter, respectively. Furthermore, the FWHM value (18 nm) for our NPs is very similar to the previously reported smallest FWHM values (18–20 nm) for the high quality CdSe NPs.[1,10] These signify that Cys-capped CdSe NPs are magic cluster NPs.

3.3. Long-Term Stability of the CdSe NPs

Figure 4 shows the time-dependent evolution of absorption spectra for the Cys-capped CdSe NPs stored at room temperature in darkness. The CdSe NPs start to show a very sharp and intense first excitonic peak from 6 days and the shape, intensity, and position for the peak experience little change with time after that. The time-dependent

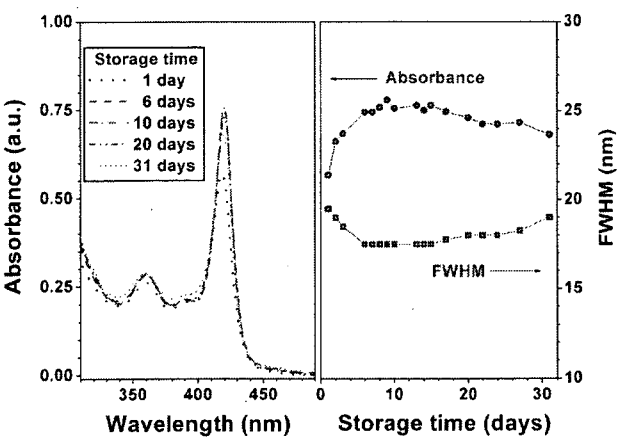

Fig. 4. (Left) Evolution of absorption spectra for Cys-capped CdSe NPs with storage time and (right) corresponding time-dependent evolution of intensity and FWHM for the first excitonic peak. The Cys-capped NPs were synthesized at the Se/Cd molar ratio of 0.25 and the Cys/Cd molar ratio of 8.8.

changes of the intensity and FWHM for the peak reveal that the peak becomes sharper with increasing peak intensity. Up to 6 days, as storage time increases, absorbance increases while FWHM decreases, indicating the growth and size-focusing of the NPs with time. Between 6 and 16 days, both absorbance and FWHM show little change, signifying the existence of stable Cys-capped CdSe NPs. After that, there observed slight decrease in absorbance and tiny increase in FWHM with storage time, insinuating the slight degradation of the NPs. However, the NPs stored for 1 month still show a very sharp first excitonic peak comparable to that for the NPs stored for 6 to 16 days, suggesting very high stability of the NPs selectively grown at a particular size in the aqueous environment.

4. CONCLUSION

Very stable and small Cys-capped CdSe NPs were synthesized directly from the basic aqueous solution at room temperature. The CdSe NPs showed a very sharp first excitonic peak at 420 nm (FWHM = 18 nm) which is very similar to that for the magic cluster CdSe NPs stabilized by hydrophobic capping molecules in organic solvents, indicating the formation of magic cluster NPs. The CdSe NPs have an excellent stability at room temperature under darkness: their absorption features experienced little change over a month, signifying their extremely high stability against time. The synthesis conditions of the CdSe NPs were very critical to their stability and optical property: only the NPs prepared at specific conditions (Se/Cd molar ratio between 0.25 and 0.5, Cys/Cd molar ratio of ~9, and solution pH of ~12) possessed an excellent stability against time and showed the typical sharp absorption spectra. Under these conditions, the peaks always appear at nearly the same wavelength, indicating that these NPs are selectively stable and grow at a particular size and structure.

Acknowledgments: This work was partially supported by Grant-in-Aid from the Ministry of Education, Science, Sports and Culture, and the Ministry of Health, Labor and Welfare, Japan.

References and Notes

1. C. M. Murray, D. J. Norris, and M. G. Bawendi, *J. Am. Chem. Soc.* 115, 8706 (1993).
2. Z. A. Peng and X. Peng, *J. Am. Chem. Soc.* 124, 3343 (2002).
3. Z. Zhelev, R. Bakalova, H. Ohba, R. Jose, Y. Imai, and Y. Baba, *Anal. Chem.* 78, 321 (2006).
4. H.-J. Choi, J.-K. Yang, and H.-H. Park, *Thin Solid Films* 494, 207 (2006).
5. D. E. Gomez, J. Embden, J. Jasieniak, T. A. Smith, and P. Mulvaney, *Small* 2, 204 (2006).
6. R. Jose, N. U. Zhanpeisov, H. Fukumura, Y. Baba, and M. Ishikawa, *J. Am. Chem. Soc.* 128, 629 (2006).
7. S. Pradhan, S. Chen, S. Wang, J. Zou, S. M. Kauzlarich, and A. Y. Louie, *Langmuir* 22, 787 (2006).
8. M. L. Steigerwald, A. P. Alivisatos, J. M. Gibson, T. D. Harris, R. Kortan, A. J. Muller, A. M. Thayer, T. M. Duncan, D. C. Douglass, and L. E. Brus, *J. Am. Chem. Soc.* 110, 3046 (1988).
9. [illegible], G. Milczarek, I. Dmitruk, Y. Barnakov, R. Czajka, S. Ryvales, X. Liu, K. Tohji, B. Jeyadevan, K. Shinoda, T. Ogawa, T. Arai, T. Hihara, and K. Sumiyama, *Colloids and Surfaces A: Physicochem. Eng. Aspects* 202, 291 (2002).
10. A. Kasuya, R. Sivamohan, Y. A. Barnakov, I. M. Dmitruk, T. Nirasawa, V. R. Romanyuk, V. Kumar, S. V. Mamykin, K. Tohji, B. Jeyadevan, K. Shinoda, T. Kudo, O. Terasaki, Z. Liu, R. V. Belosludov, V. Sundararajan, and Y. Kawazoe, *Nature Materials* 3, 99 (2004).
11. J. Aldana, Y. A. Wang, and X. Peng, *J. Am. Chem. Soc.* 123, 8844 (2001).
12. R. Hong, N. O. Fischer, A. Verma, C. M. Goodman, T. Emrick, and V. M. Rotello, *J. Am. Chem. Soc.* 126, 739 (2004).
13. D. V. Talapin, A. L. Rogach, I. Mekis, S. Haubold, A. Kornowski, M. Haase, and H. Weller, *Colloids and Surfaces A: Physicochem. Eng. Aspects* 202, 145 (2002).
14. A. L. Rogach, A. Kornowski, M. Gao, A. Eychmüller, and H. Weller, *J. Phys. Chem. B* 103, 3065 (1999).
15. Y. J. Yang and B. J. Xiang, *J. Crystal Growth* 284, 453 (2005).
16. X. Zhou, Y. Kobayashi, N. Ohuchi, M. Takeda, and A. Kasuya, *Int. J. Mod. Phys. B* 19, 2835 (2005).
17. X. Zhou, Y. Kobayashi, V. Romanyuk, N. Ohuchi, M. Takeda, S. Tsunekawa, and A. Kasuya, *Appl. Surf. Sci.* 242, 281 (2005).
18. V. Ptatschek, T. Schidt, M. Lerch, G. Müller, L. Spanhel, A. Emmerling, J. Fricke, A. H. Foitzik, and E. Langer, *Ber. Bunsenges. Phys. Chem.* 102, 85 (1998).

Received: 26 April 2007. Revised/Accepted: 5 June 2007.

Int J Clin Oncol (2008) 13:12–17
DOI 10.1007/s10147-007-0723-5

REVIEW ARTICLE

Takanori Ishida · Motohiro Takeda · Akihiko Suzuki
Masakazu Amari · Takuya Moriya · Noriaki Ohuchi

Significance of irradiation in breast-conserving treatment: comparison of local recurrence rates in irradiated and nonirradiated groups

Received: September 3, 2007

Abstract Breast-conserving treatment (BCT) is a standard therapy for early breast cancer. Many reports have described the effectiveness of post-BCT radiation therapy. However, the post-BCT local recurrence rate of only 5% to 10% indicates that radiation therapy may be unnecessary in many cases. To accurately select those patients who do not require post-BCT radiation therapy, we investigated the significance of irradiation in BCT by comparing local recurrence rates in irradiated and nonirradiated patients, grouped according to clinicopathological criteria that we evaluated. The patients were divided into two groups: a previous-criteria group and a present-criteria group. The former group included 85 patients in whom only two factors were considered as the criteria for radiation therapy: margin-positivity and lymphatic metastasis-positivity. The latter group included 318 patients in whom three additional factors were also considered: lymphatic invasion, intraductal extension, and metachronous/synchronous bilateral breast cancer. The use of five clinicopathological factors rather than two as the criteria for irradiation led to an increase in the irradiation ratio from 47.1% to 63.2% and a decrease in local recurrence from 12.9% to 2.2%. Because of the short average follow-up period of this study, further careful, regular follow-up and randomized comparative studies are required. It may also be necessary to include the patient age and margin condition as mandatory criteria for irradiation.

Key words Breast cancer · Breast-conserving treatment (BCT) · Radiation therapy

Introduction

Breast-conserving treatment (BCT) has become a common option for breast cancer treatment in Japan, and patients can now obtain substantial information through the internet and other sources. Prior to treatment, medical experts are obliged to provide patients with detailed information regarding aspects of treatment, such as indications, procedures, and outcome. The recent results of BCT at Japanese medical institutions should also be used to supplement the overseas results when explaining the treatment to patients.

Our department introduced BCT as an optional treatment in 1990. Since then, we have treated approximately 500 patients with BCT and experienced gradual changes in its indications and procedures. One of the features of our protocol modified since the introduction of BCT is the application of postoperative irradiation selectively only to a group with recurrence risks determined according to clinicopathological factors.[1–3] In light of the approximately 5% rate of local recurrence, we believe that irradiation may be unnecessary in some patients, for the following reasons: (1) not every residual cancer cell is radiation-responsive; (2) in hormone-responsive tumors, hormone administration provides effective prevention of local recurrence; (3) eliminating postoperative irradiation can reduce the financial burden on the patient; (4) there are large regional differences in the radiation therapy equipment of medical institutions; and (5) latent disorders and other effects of radiation have not yet been fully elucidated.

We herein describe a comparison of the outcomes in an irradiated group versus a nonirradiated group, while also discussing the relationship between the outcome and clinicopathological factors used as criteria for irradiation.

T. Ishida (✉) · M. Takeda · A. Suzuki · M. Amari · N. Ohuchi
Division of Surgical Oncology, Tohoku University School of Medicine, 1-1 Seiryo-machi, Aoba-ku, Sendai 980-8574, Japan
Tel. + 81-22-717-7214; Fax + 81-22-717-7217
e-mail: takanori@mail.tains.tohoku.ac.jp

T. Moriya
Second Department of Pathology, Kawasaki Medical School, Kurashiki, Japan

Patients and methods

Patients

We investigated 403 patients who received BCT at the Division of Surgical Oncology, Tohoku University School of Medicine, from September 1990 to December 2004. Table 1 summarizes the clinicopathological factors. By age, 46 patients (11.4%) were below 40 years, 241 (59.8%) were between 40 and 60 years, and 116 (28.8%) were 61 years and older. Histologically, 59 patients (14.7%) had ductal carcinoma in situ (DCIS), 304 (75.4%) had invasive ductal carcinoma (IDC), and 40 (9.9%) had other types of carcinoma, such as lobular carcinoma. According to tumor size, 59 patients were stage Tis (14.7%), and 211 were T1 (52.3%), the sum of which accounted for more than half of the subjects. The remaining 133 patients were T2 (33.0%). Patients with neoadjuvant chemotherapy were not enrolled in this study.

Indications for breast-conserving therapy (BCT)

The indication for BCT as of September 1990, when we introduced BCT, consisted of a "tumor in diameter (tumor size) of 3 cm or less, no metastasis to axillary lymph node, without multifoci involving several quadrants or extensive fine calcification" as shown in Table 2.

Subsequently we introduced preoperative three-dimensional diagnostic imaging; for example, dynamic magnetic resonance imaging (MRI) in 1995 and helical computed tomography (CT) in 2000, followed by intraoperative rapid pathological diagnosis in all patients.[4] The present indications for BCT are therefore as follows: "A tumor with a diameter of 3 cm or less, in principle. In addition the surgical margin is likely to become cancer-negative, and the cosmetic outcome will be acceptable in spite of the findings of extensive cancer or multifoci by diagnostic imaging. Metastasis to the axillary lymph nodes, nipple discharge, tumor site, and the distance from tumor to nipple are irrelevant."

The reasons for the expanded indications included the following: (1) the local recurrence rate was approximately 5%; (2) the use of three-dimensional diagnostic imaging such as MRI and CT in combination with mammography and ultrasonography enabled a more accurate preoperative diagnosis of the extensive intraductal components and multifoci;[4] and (3) the pathologists at our facility specializing in breast disease provided a positive diagnosis of 95% or more in intraoperative rapid pathological diagnoses.

Postoperative adjuvant treatment

Postoperative irradiation

When we started BCT, the indications for irradiation consisted of metastasis to the axillary lymph node(s) and/or a positive surgical margin (Table 2), and 47.1% of patients receiving BCT underwent postoperative irradiation. A subsequent investigation of local recurrence suggested that 2 cm or more of intraductal extension, positive ly- factor, and/or metachronous/synchronous bilateral breast cancer should also be regarded as indications for postoperative irradiation. As a result of the expanded indications for postoperative irradiation (Table 3) in 1997, 63.2% of the patients treated with BCT underwent postoperative irradiation.

The standard radiation dose in all conserved breasts has been 50 Gy since the introduction of BCT, with the exception that 10 Gy is added to boost the irradiation to the surgical margins. This dosage has remained unchanged.

Table 1. Patient and tumor characteristics

	Patients (n = 403)	
	Previous-criteria (n = 85)	Present-criteria (n = 318)
Age (years)		
<40	13	33
40–60	57	184
>60	15	101
Histology		
Ductal carcinoma in situ	6	53
Invasive ductal carcinoma	70	234
Other (lobular carcinoma, etc.)	9	31
Tumor stage		
Tis	6	53
T1	52	159
T2	27	106
Margin status		
Positive	17	66
Negative	68	252
Positive nodes		
0	65	244
1–3	16	47
≧4	4	27

Table 2. Tohoku University Breast-Conserving Therapy Research Group Protocol (summary, 1990–1996 criteria)

1. Breast-conserving surgery
   (1) Indication: stages Tis, I and II (T ≤ 3.0 cm, no metastasis to axillary lymph node(s)), without multifoci involving several quadrants or extensive fine calcification
   (2) Lesion site: any
   (3) Resection: quadrantectomy (Bq 90°, 3 cm) in principle
      (a) Skin excision immediately above the tumor in a width more than the tumor radius (Tumor size)
      (b) Skin incision for quadrantectomy and axillary dissection done simultaneously for tumor in upper outer quadrant; otherwise done separately
      (c) Remove a safe margin 2 cm or wider from the tumor margin
      (d) Perform intraoperative specimen mammography for T0 cases with fine calcification

2. Radiation therapy (previous criteria)
   (1) Indication: satisfaction of at least one of the following requirements:
      (a) Lymphatic metastasis-positive
      (b) Margin-positive (cancer lesion exists within 5 mm from surgical margin)
   (2) Dose: 50 Gy. Total of 60 Gy when boost dose to surgical margin is required

Table 3. Tohoku University Breast-Conserving Therapy Research Group Protocol (Summary, 1997–2004 criteria)

1. Breast-conserving surgery
   (1) Indication: stages 0, I and II (T ≤ 3.0 cm; metastasis to axillary lymph node(s) is irrelevant), without high grade of intraductal carcinoma extension or multifoci involving several quadrants by diagnostic imaging
   (2) Lesion site: any
   (3) Resection: quadrantectomy (Bq 90°, 3 cm), in principle
      (a) Without skin excision, in principle
      (b) Skin incision from the apex of the mid-axillary line to the inframammary skin fold (lateral incision) is used for tumor at any site
      (c) Remove a safe margin, 2 cm or wider from the tumor margin
      (d) Intraoperative specimen mammography and rapid margin evaluation to be performed by the pathology laboratory

2. Radiation therapy (present criteria)
   (1) Indication: satisfaction of at least one of the following requirements:
      (a) Lymphatic metastasis-positive or advanced lymphatic invasion (ly 2+, 3+)
      (b) Margin-positive (cancer lesion exists within 5 mm from surgical margin)
      (c) High grade of intraductal carcinoma extension (2 cm or more)
      (d) Metachronous/synchronous bilateral breast cancer
   (2) Dose: 50 Gy. Total of 60 Gy when boost dose to surgical margin is required

Chemoendocrine therapy

Since 1990 we have applied our own regimen of chemoendocrine therapy, depending mainly on the presence of lymph node metastasis. Our present application is, however, an evidence-based protocol. For example, according to the St. Gallen treatment recommendations, we considered clinicopathological risk factors such as the presence of metastasis to the lymph node(s), premenopausal/postmenopausal onset, tumor size, hormone receptors, and histological grade.[5]

It should be noted that we previously prescribed antiestrogens without performing any receptor examination in patients with a small tumor size, thus leaving the receptor levels unknown. In 1997 we also began to perform receptor level analyses, with immunohistochemical staining, on a trial basis, and in 2000 we made such analyses a routine determinant for endocrine therapy in every patient.

Purpose and methods

We sought to investigate the effect of postoperative irradiation on local recurrence in irradiated and nonirradiated BCT groups and to elucidate the clinicopathological factors that were pertinent as indications for postoperative irradiation. This will allow us to select those patients who require no postoperative irradiation, thus allowing patients who are not expected to benefit from BCT to avoid such treatment, thereby reducing costs and also preventing unnecessary side effects.

The 403 patients investigated were divided into two groups: consisting of a previous-criteria group of 85 patients and a present-criteria group of 318 patients. Specifically, our decision to perform postoperative irradiation was based on our 1990–1996 criteria (Table 2) in the former group and on our 1997–2004 criteria (Table 3) in the latter group. Our study focused on the correlation between ipsilateral breast cancer recurrence and the clinicopathological factors in each group.

Results

Among the 85 previous-criteria patients, 40 patients (47.1%) underwent irradiation in the conserved breast and 45 patients (52.9%) did not. Recurrence was observed in 3

patients (7.5%) in the irradiated group and in 8 patients (17.8%) in the nonirradiated group; this difference was not significant, but the recurrence rate was higher in the nonirradiated group (Table 4). The median follow-up period was 166 months. Therefore, we further investigated the 8 nonirradiated patients in the previous-criteria group with recurrence in terms of the clinicopathological factors (Table 5). Pathological examination revealed 2 cm or more intraductal carcinoma extension in 3 patients, advanced lymphatic invasion in 2 patients, and metachronous bilateral breast cancer in 2 patients. Ipsilateral breast cancer recurrence occurred 15 to 128 months (median, 54 months) after the first surgery. In all but 1 patient, these recurrences were observed in younger patients, aged 60 years or less at the time of surgery.

Based on these results, in 1997 we changed the indications for postoperative irradiation. According to these criteria (present criteria), postoperative irradiation is indicated if at least one of the following requirements is met: advanced lymphatic invasion, extensive intraductal component (2 cm or more), or metachronous/synchronous bilateral breast cancer. These indications are, of course, additional to the previous indications, i.e., positive margin (within 5 mm) and positivity for lymphatic metastasis (Table 3). Consequently, 201 of 318 patients (63.2%) in the present-criteria group underwent irradiation and 117 patients (36.8%) did not. Ipsilateral breast cancer recurrence was observed in 6 patients (3.0%) in the irradiated group and in 1 patient (0.8%) in the nonirradiated group; this difference was not significant (Table 6). The median follow-up period in the present-criteria group was 70 months.

Among the total cohort of 403 patients, 116 patients (28.8%) were aged 61 years or older. Of these 116 patients, 55 underwent irradiation according to our own criteria, and 61 did not. Only 1 of these 116 patients developed a local recurrence. Among the 55 irradiated patients, 36 (65.5%) were margin-negative and estrogen receptor-positive.

Among the total cohort of 403 patients, 83 (20.6%) were margin-positive. Our definition of a "positive margin" is the finding of a cancerous lesion within 5 mm of the resection margin when the resected specimen is completely sectioned (section width of 5 mm) and pathologically examined. Seventeen patients in the previous-criteria group and 66 in the present-criteria group were margin-positive; all 83 patients underwent irradiation in the conserved breast. Of the 17 patients in the previous-criteria group, 2 developed local recurrence, in which a cancerous lesion was found on the surgical margin. Of the 66 patients in the present-criteria group, 3 patients developed local recurrence, in which a cancerous lesion was also found on the surgical margin.

Discussion

It is well known that radiation therapy subsequent to BCT can prevent the local recurrence of cancer.[6-9] However, the local recurrence rate of, at most, 5% is an obvious indication of a patient group undergoing essentially unnecessary radiation therapy. Moreover, not every residual cancer cell is radiation-responsive, and there are currently no established methods for determining such responsiveness.

Table 4. Ipsilateral breast recurrences in previous-criteria group

	Patients ($n = 85$)	Ipsilateral breast recurrence	Recurrence rate (%)
Irradiated group	40	3	7.5
Nonirradiated group	45	8	17.8*

*NS

Table 6. Ipsilateral breast recurrences in present-criteria group

	Patients ($n = 318$)	Ipsilateral breast recurrence	Recurrence rate (%)
Irradiated group	201	6	3.0
Nonirradiated group	117	1	0.8*

*NS

Table 5. Patients with local recurrence after BCT with no radiation therapy

Patient no.	Age at primary operation (years)	Time from primary operation to local recurrence (months)	Features of histopathology
1	45	54	High grade of ductal spreading[a]
2	54	48	High grade of ductal spreading
3	44	15	Metachronous bilateral breast cancer
4	55	73	ly ++[b]
5	60	74	With no particular features[c]
6	41	23	ly +++
7	60	54	High grade of ductal spreading
8	49	128	Metachronous bilateral breast cancer

[a] High grade means that intraductal carcinoma component extends over 2 cm
[b] ly, lymph vessel invasion
[c] Second primary cancer suspected

It has also been reported that hormonal drugs act on hormone-responsive tumors, effectively preventing a local recurrence.[10,11] These facts suggest that patients who require no radiation therapy could be screened out and thereby spared an unnecessary financial and physical burden.

There is also the problem of the large regional differences in the availability of radiation therapy facilities. Patients who cannot find a radiation therapy facility locally must remain overnight in a hospital far from home to receive the necessary treatment, which thus presents a heavy financial and psychological burden. If hospital treatment is impossible, the patient cannot receive the benefit of BCT even when desired. The elimination of such disadvantages is one of the main purposes of our efforts to select patients requiring no radiation therapy.

From the time we introduced BCT, our protocol has stressed the assurance of a safe surgical margin and the minimization of residual cancer cells.[1-3]. Not every cancer cell is responsive to radiation, and we feel that the most important factor for preventing recurrence is the surgical assurance of cancer-negative margins, as described by Smitt et al.[12]

We have also investigated the pathological development and progression of breast cancer with three-dimensional imaging for many years, reporting that breast cancer typically originates from a peripheral lactiferous duct and then spreads along the lobules of the mammary gland towards the large duct or infiltrates into the interstitial tissues.[1,13,15] Pathological examination of the resected specimens has shown an extensive intraductal component toward the nipple in many patients. The prevention of residual cancer thus requires elimination of the anatomical system of lobules of the mammary gland up to a point immediately beneath the nipple, which is why we insist on quadrantectomy. On this basis, our standard procedure is quadrantectomy by tumor excision with 3-cm free margins.[15]

We also investigated clinicopathological factors such as lesion size by a post-BCT precise pathological examination of the resected specimens. Since our introduction of BCT, we have developed a pathological map for each patient by fixing the resected specimen with formaldehyde and sectioning the whole specimen 3-mm- to 5-mm-thick with a microtome to prepare a pathological specimen.[15] We investigate the clinicopathological characteristics of the specimens in detail for characteristics including the histological type, lesion depth, intraductal extension, multifoci, grade, distance from the margin, ly- and v-factors, histological grade, lymph node metastasis, and responsiveness to hormones. We use the results to determine the postoperative adjuvant treatment such as radiation therapy and chemoendocrine therapy. Furthermore, we have applied intraoperative specimen mammography to the mammary gland to be resected in all patients since 1994 to ensure a more accurate, safer resection area. The aim is to confirm that the main tumor is centered in the resection area and that, if microcalcification is found, to ensure that it is completely within the resection area. If the resection area is observed to have shifted either laterally or toward the papilla, then we resect an additional mammary gland in that direction.

We also use three-dimensional diagnostic imaging for the preoperative examination. Specifically, we introduced dynamic MRI in 1995 and helical CT in 2000. These modalities are excellent for depicting an extensive intraductal component and multifoci. A computer-aided three-dimensional graphical presentation allows us to make the preoperative diagnosis visually. The additional use of three-dimensional imaging is effective for determining whether BCT is indicated and for setting a suitable resection area.

We feel that an intraoperative margin evaluation is also an important factor for safely performing BCT. Previously, a rapid margin evaluation was performed only in limited, selected patients. Since 1997, such a margin evaluation has been performed for all patients by the pathology laboratory. We prepare a margin specimen for evaluation with a shears to avoid thermal degeneration, and then send the margin from the conserved breast after a quadrantectomy to the laboratory. Though the reliability of intraoperative rapid diagnosis is controversial, our hospital has the advantage of having capable pathologists on staff who specialize in breast diseases; our correct diagnosis rate is thus greater than 95%. The remaining 5% is an overdiagnosis of proliferative lesions suspected of being cancer. There is no underdiagnosis of margin-positive patients proven by permanent specimen evaluation that contradicts a margin-negative intraoperative pathological diagnosis.

It should be noted that the Japanese Breast Cancer Society's guidelines for BCT recommend that if a lesion is found within 5 mm of the margin, the case should be judged as cancer-positive. The underlying idea is that if a lesion is found adjacent to the surgical margin, it should be regarded as cancer-positive, while taking specimen preparation errors into account.

It has been reported that the surgical assurance of negative margins is an important factor in local recurrence prevention. In our study, we observed local recurrence in 5 of the 83 margin-positive patients (6.0%) and 13 of the 320 margin-negative patients (4.1%). There was no significant difference between these two groups. However, in the 5 margin-positive patients with recurrence, the lesions were observed just on the surgical margin, thus suggesting that these lesions were poorly controlled by radiation therapy.

Our initial criteria for postoperative radiation therapy consisted of just two factors: margin-positivity (within 5 mm) and lymphatic metastasis-positivity. The local recurrence rate in the group with our initial criteria for postoperative radiation therapy was 7.5% in the irradiated group and 17.8% in the nonirradiated group. This difference was substantial, but not significant. Based on this finding, we modified the criteria by adding three additional factors: advanced lymphatic invasion, extensive intraductal component (2 cm or deeper), and metachronous/synchronous bilateral breast cancer. According to the modified criteria, when at least one of these five requirements was met, the patient was classified in the irradiated group. Consequently, 63.2% of all patients were classified in the irradiated group, compared with 47.1% before the criteria modification. However, after the criteria modification, a local recurrence occurred in 6 patients in the irradiated group, and in 1 in the nonir-

radiated group. Because the median follow-up period after the criteria modification has been only 70 months, with a maximum of 127 months, further long-term follow-up is required. Nonetheless, we have thus far observed no difference between the irradiated and the nonirradiated groups.

Another point to be considered as a factor related to local recurrence is patient age. Of the 403 studied patients, 116 (28.8%) were aged 61 years or above. Only 1 of these 116 patients developed an ipsilateral breast cancer recurrence. Among these 116 patients, 55 received radiation therapy according to our criteria for irradiation, and 36 of these patients were margin-negative and estrogen receptor-positive. These results suggest that hormonal therapy alone may be sufficient to prevent local recurrence if a patient is older than 60 years and is also both margin-negative and hormone receptor-positive. Currently, several medical institutions are involved in a randomized comparative study of the elimination of radiation therapy in such patients. Future analyses are also eagerly awaited.

Conclusions

Based on the following clinicopathological characteristics: (1) lymphatic metastasis-positivity, (2) advanced lymphatic invasion (ly 2+, 3+), (3) margin-positivity (the cancer lesion exists within 5 mm of the surgical margin), (4) a high grade of intraductal carcinoma extension (2 cm or more), and (5) metachronous/synchronous bilateral breast cancer, we divided the studied patients into an irradiated group and a nonirradiated group for the purpose of selecting the patients with breast cancer in whom post-BCT radiation therapy could be eliminated. Only 1 (0.8%) local recurrence has occurred in the nonirradiated group since the start of case selection according to our present, five-factor-based criteria. However, the follow-up period in this study is still not sufficiently long, and further regular, careful follow-up and multicenter randomized comparative studies are thus required.

In cooperation with several medical institutions, we plan to perform another randomized comparative study on the elimination of radiation therapy according to our present, five-factor-based criteria for radiation therapy. The results of these studies are expected to contribute to the establishment of safer, simpler BCT that should be able to benefit more patients.

References

1. Ohuchi N (1999) Breast-conserving surgery for invasive cancer: a principle based on segmental anatomy. Tohoku J Exp Med 108: 103–118
2. Ohuchi N, Harada Y, Ishida T, et al. (1997) Breast-conserving surgery for primary breast cancer: immediate volume replacement using lateral tissue flap. Breast Cancer 4:135–141
3. Ohuchi N, Furuta A, Mori S (1994) Management of ductal carcinoma in situ with nipple discharge. Cancer 74:1294–1302
4. Amano G, Ohuchi N, Ishida T, et al. (2000) Correlation of three-dimensional magnetic resonance imaging with precise histopathological map concerning carcinoma extension in the breast. Breast Cancer Res Treat 1638:1–13
5. Goldhirsch A, Wood WC, Gelber RD, et al. (2007) Progress and promise: highlights of the international expert consensus on the primary therapy of early breast cancer 2007. Ann Oncol 18: 1133–1144
6. Fisher B, Anderson S, Redmond CK, et al. (1995) Reanalysis and results after 12 years of follow-up in a randomized clinical trial comparing total mastectomy with lumpectomy with or without irradiation in the treatment of breast cancer. N Engl J Med 333: 1456–1461
7. Veronesi U, Marubini E, Mariani L, et al. (2001) Radiotherapy after breast-conserving surgery in small breast carcinoma; long-term results of a randomized trial. Ann Oncol 12:997–1003
8. Liljegren G, Holmberg L, Bergh J, et al. (1999) Ten-year results after sector resection with or without postoperative radiotherapy for stage I breast cancer; a randomized trial. J Clin Oncol 17: 2326–2333
9. Clark RM, Whelan T, Levine M, et al. (1996) Randomized clinical trial of breast irradiation following lumpectomy and axillary dissection for node-negative breast cancer; an update. J Natl Cancer Inst 88:1659–1664
10. Fisher B, Dignam J, Wolmark N, et al. (1999) Tamoxifen in tratment of intraductal breast cancer: National Surgical Adjuvant Breast Project (NSABP) Protocol B-24 randomized controlled trial. Lancet 353:1993–2000
11. Fisher B, Dignam J, Bryant J, et al. (1996) Five versus more than 5 years of tamoxifen therapy for breast cancer patients with negative lymph nodes and estrogen receptor-positive tumors. J Natl Cancer Inst 88:1529–1542
12. Smitt MC, Nowels KW, Zdeblick MJ, et al. (1995) The importance of the lumpectomy surgical margin status in long term results of breast conservation. Cancer 76:259–267
13. Ohuchi N, Abe R, Kasai M (1984) Possible cancerous change of intraductal papillomas of the breast: a 3-D reconstruction of 25 patients. Cancer 54:605–611
14. Page DL, Anderson TJ, Rogers LM (1987) Epithelial hyperplasia. In: Page DL, Anderson TJ (eds) Diagnostic histopathology of the breast. Churchill Livingstone, Edinburgh, pp 120–156
15. Ishida T, Furuta A, Moriya T, et al. (2003) Pathological assessment of intraductal spread of carcinoma in relation to surgical margin state in breast-conserving surgery. Jpn J Clin Oncol 33:161–166

Fluorescence Tomography of Biological Tissue Based on Ultrasound Tagging Technique

Masaki Kobayashi*[a], Takashi Mizumoto[a], Trinh Quang Duc[a], Motohiro Takeda[b, c]
[a] Department of Electronics, Tohoku Institute of Technology, Sendai 982-8577, Japan;
[b]Department of Bioengineering and Robotics, Graduate School of Engineering, Tohoku University, Sendai 980-8579, Japan; [c]Division of Surgical Oncology, Graduate School of Medicine, Tohoku University, Sendai 980-8579, Japan

ABSTRACT

We report a study for the development of tomographic imaging technique of fluorescence in biological tissue for assays of biological function. Ultrasonic modulation of light based on the acousto-optic effect (so called ultrasound 'tagging') is applied for imaging of fluorescence distribution in the light-scattering media. Sound-field characteristics that affect the light by modulating its amplitude through variation of the refractive index in the medium were determined. With using focused ultrasound, selectively modulated fluorescence on a depth-axis of the medium can be detected. Ultrasound tagging technique applied measuring the optical absorption in light scattering media is well known, and it is principally based on the modulation of speckle pattern. On the contrary, in the case of fluorescence, displacement of scattering particles and variation of the refractive index that is induced by density distribution in a sound field might produce the intensity modulation of scattered light. We have experimentally shown that ultrasound tagging technique is also available for fluorescence measurement. In this paper, we demonstrate the result of tomographic images of fluorescence in dense scattering media using porcine muscle as a biological tissue, and bovine adipose. Tissue samples had the dimension of 40 x 40 mm in section and fluorophore which had the 3mm size was embedded in the center of the tissue. The localized image of the fluorophore was determined with the spatial resolution of focus size of the ultrasound, suggesting the applicability of this technique for visualization of fluorescent probes in deep portion of living body.

Keywords: fluorescence , imaging, acoustooptic effect, ultrasound, laser, tomography, turbid medium, scattering

1. INTRODUCTION

Fluorescence imaging techniques for the analysis of biological functions using fluorescent probes that label physiological molecules are an essential tool in the field of life science. Recently, quantum dots, which have excellent optical performance, have been widely used as new fluorescent probes, and are also anticipated to be applied for clinical use. Fluorescent probes for bioassay have the advantage of dynamics visualization of bio-functions in real-time with low invasion. However, the light-scattering in biological tissues restricts the applicability of fluorescence imaging of living bodies inside. A great deal of effort has been devoted to develop the optical imaging technique for living bodies [1]. Those efforts have made improve the technique of characterization of optical properties even in light scattering media. Recently, the 'tagging' technique using the interaction of light with ultrasound has been widely studied for exploring the novel technique to determine the optical absorption in biological tissue [2]. In the case of absorption determination using tagging technique, the intensity modulation in a varying sound-pressure field is caused by the variation of speckle pattern formed in multiply scattered coherent light. We have examined the feasibility of the application of tagging technique for fluorescence imaging. In the case of fluorescence, the displacement of scattering particles and variation of the refractive index induced by density distribution in a sound field might also generate the intensity modulation [3]. We have already demonstrated the availableness of this technique for fluorescence imaging with using tissue phantoms under the condition of 532nm excitation [4]. Here, we demonstrate tomographic imaging of fluorescence in biological tissue in which fluorofore is locally embedded in the center of the tissue.

* masaki@tohtech.ac.jp; phone 81 22 305-3211; fax 81 22 305-3202

Biophotonics 2007: Optics in Life Science, edited by Jürgen Popp, Gert von Bally, Proc. of SPIE-OSA Biomedical Optics, SPIE Vol. 6633, 663306, © 2007 SPIE-OSA · 1605-7422/07/$18

2. MATERIALS AND METHODS

2.1 Experimental setup

Figure 1 shows that the experimental setup. A continuous wave (CW) Ti:sapphire laser system pumped with a diode pumped solid state (DPSS) laser (Verdi V-6; Coherent Inc.) is used as light source for excitation. The laser beam is reduced and collimated, and goes through the glass window on the side wall of a water tank. A focus-type ultrasonic transducer (38 mm focal length, 3 mm focal diameter, V314-SU; Olympus-NDT) that is driven by a 1 MHz continuous sinusoidal wave is incorporated into the side wall of the water tank, where the ultrasound beam traverses the incident axis of the laser beam. Sound pressure in the sound-field focus region was 4.1×10^4 Pa in water. A photomultiplier tube (PMT) is placed by the opposite side of the window of incident beam. The signal from the PMT is fed into a spectrum analyzer and the intensities of the resonant frequencies are detected using a narrow bandwidth (100Hz). To obtain a two-dimensional tomographic image of fluorescence intensity through scanning of the ultrasound focus, a water tank equipped with a transducer is mounted on a three-axis translational stage and scanned in 500 μm steps along the X-axis (parallel to the incident laser beam) and the Y-axis (parallel to the ultrasound beam). Total scanning area is 20 × 20 mm. It is controlled using a personal computer via GP-IB interface that is synchronized with a spectrum analyzer. The entire control program was written in Lab windows (National Instruments Co., USA).

A sample for the measurement (tissue phantoms or biological tissues) is put in an acrylic holder and suspended from the outside of the water tank. The sample with acrylic holder is immersed in the water. The optical arrangement of the sample and incident laser beam remains unchanged during scanning of the ultrasound beam which is from the side wall of the water tank. The imaging experiments are conducted using a wavelength of 726 nm and an incident beam signal intensity of 40 mW. The light modulation mechanism is inferred to be induced through density variation of the medium in the ultrasound field, which engenders changes of the refractive index and optical scattering coefficient. When fluorescent pigment is present in the sound field, the density variation of the medium engenders modulation of the photon density through deflection of light between two successive scattering events in the gradient of the refractive index, thereby causing fluorescence intensity modulation. Variation of the scattering coefficient may also cause modulation of the fluorescence intensity.

Characteristics of fluorescence modulation intensity as a function of sound pressure measured under the condition in which ultrasound focuses on the fluorescent region site in the scattering medium shows that fluorescence modulation (signal) intensity is proportional to the square of the sound pressure, indicating a linear relationship between the sound power and the fluorescence signal intensity [4].

2.2 Sample

As a tissue phantom, we fabricated isotropic light-scattering gel made of 5% agar (Inagel; Ina Food Industry Co. Ltd., Nagano, Japan) that were prepared through dilution of Intralipid (Intralipid-10%; Fresenius Kabi AG, Germany). The final volume concentration of Intralipid in the phantom was 80 ml/l in 5% agarose gel with the water-glycerin (20%) solution. The agarose gel was molded to 40 × 40 × 75 (height) mm. A fluorescent region in the phantom was formed by embedding a fluorescent material that contains fluorescent microspheres (715 nm absorption peak, 755 nm emission wavelength; carboxylate-modified microspheres, FluoSheres F-8799, Molecular Probes Inc., USA) molded with columnar agarose gel (5 mm long, 3 mm diameter).

A tissue of porcine muscle purchased from a supermarket is used as a biological tissue sample. It is cut and formed with 40 × 40 × 75 mm, and drilled at the center of the tissue. Fluorescent microspheres (FluoSheres F-8799) molded with columnar capsule (5 mm long, 3 mm diameter) is embedded in the center of the tissue.